Splattering and Heat Transfer During Impingement of a Turbulent Liquid Jet

J. H. Lienhard V
Associate Professor.
Mem. ASME

X. Liu
Research Assistant.
Student Mem. ASME

L. A. Gabour
Research Assistant.

Department of Mechanical Engineering,
Massachusetts Institute of Technology,
Cambridge, MA 02139

Splattering and heat transfer due to impingement of an unsubmerged, fully turbulent liquid jet is investigated experimentally and analytically. Heat transfer measurements were made along a uniformly heated surface onto which a jet impacted, and a Phase Doppler Particle Analyzer was used to measure the size, velocity, and concentration of the droplets splattered after impingement. Splattering is found to occur in proportion to the magnitude of surface disturbances to the incoming jet, and it is observed to occur only within a certain radial range, rather than along the entire film surface. A nondimensional group developed from inviscid capillary disturbance analysis of the circular jet successfully scales the splattering data, yielding predictive results for the onset of splattering and for the mass splattered. A momentum integral analysis incorporating the splattering results is used to formulate a prediction of local Nusselt number. Both the prediction and the experimental data reveal that the Nusselt number is enhanced for radial locations immediately following splattering, but falls below the nonsplattering Nusselt number at larger radii. The turbulent heat transfer enhancement upstream of splattering is also characterized.

1 Introduction

Liquid jets are often directed onto hot surfaces to provide simple and efficient cooling. Such jets typically issue from a nozzle at the terminus of a pipe, or similar manifolding system, and may be encountered in a wide range of manufacturing, laser-heated, or electronic systems. Quenching of steels during rolling processes, or, conversely, cooling of the rollers themselves during hot rolling, are just two common examples. Circular liquid jets are of particular value in creating extremely high heat transfer coefficients over relatively localized areas. The corresponding piping systems have the added attraction of being inexpensive and easy to install.

In our previous papers (Liu and Lienhard, 1989; Liu et al., 1991), we discussed the heat transfer characteristics of an unsubmerged, impinging laminar liquid jet issuing from a sharp-edged orifice. In the latter paper, disturbances to the experimental liquid supply were carefully damped so as to create uniform-velocity profile, laminar jets having very stable, undisturbed free surfaces. While that configuration is well suited for examining the physical mechanisms of jet impingement cooling, in applications such as those mentioned above, the piping or manifolding systems are likely to generate turbulence in the liquid supply. The resultant liquid jets are turbulent and have heavily disturbed surfaces, which make them susceptible to the highly undesirable effect of splattering after they strike the target surface (Fig. 1).

When a jet splatters, much of the incoming liquid can become airborne, as droplets, within a few jet diameters of the point of impact. Airborne liquid no longer contributes to the cooling of the liquid surface, and in consequence, cooling is far less efficient than it could be if splattering were suppressed. Understanding the causes and scaling of splattering is thus an essential element in jet cooling system design.

The basic physical mechanism of splattering has been described by Errico (1986). Disturbances to the surface of the incoming jet are strongly amplified as the jet spreads into a liquid film along a wall normal to the axis of the jet (Fig. 1*b*, *c*). The associated flow regimes along the surface can be characterized in an average sense as follows (Fig. 2):

1 *Stagnation Zone*: A very thin wall boundary layer with a turbulent free stream above it.
2 *Region Before Splattering*: Disturbances to the liquid sheet are strongly amplified in this region. As in the stagnation zone, the wall boundary layer is affected by turbulent and capillary disturbances to the flow above it.
3 *Region of Splattering*: A portion of the liquid sheet breaks free as droplets, owing to the instability of the disturbed liquid sheet. The effective radial size of this zone is fairly small.
4 *Region After Splattering*: Having lost both mass and momentum in the splattering process, the remaining liquid sheet continues to flow outward. The liquid sheet is fully turbulent.

Errico's experiments on the splattering of impinging jets demonstrated that jet splatter is directly tied to the surface roughness or deformation of the incoming liquid jet, that jet splatter is reduced by making the jet shorter (so that disturbances to the liquid jet have less time to develop), and that jet stability is related to the specific nozzle design. Errico also found that onset of splattering in jets forced at their breakup frequency varies with Re_d, We_d, and the ratio of jet length to jet diameter.

Splattering and turbulence both produce additional mixing in the liquid sheet, which will tend to enhance heat transfer relative to a laminar sheet. Conversely, the wall friction will be generally lower for laminar flow, which should result in larger velocities at a given downstream radius. The relative cooling efficiency of these cases is not obvious *a priori*, apart from the expectation that turbulence enhances heat transfer in the stagnation zone. Additionally, turbulence and splattering are closely related, with splattering both being driven by turbulence and adding fluctuating disturbances to the film, so that these effects must be accounted for simultaneously in attempting to model the heat removal. Presumably, the jet Reynolds and Weber numbers will appear as controlling parameters.

Since the initial condition of the jet and the subsequent flow

Contributed by the Heat Transfer Division and presented at the 27th National Heat Transfer Conference, Minneapolis, Minnesota, July 27–29, 1991. Manuscript received by the Heat Transfer Division April 1, 1991; revision received July 31, 1991. Keywords: Forced Convection, Jets, Sprays/Droplets.

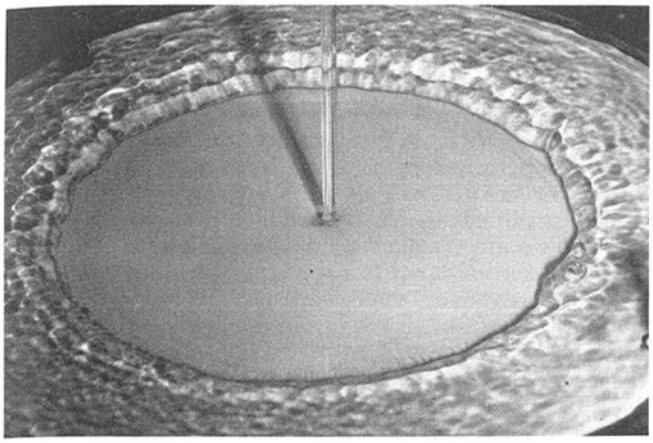

(a)

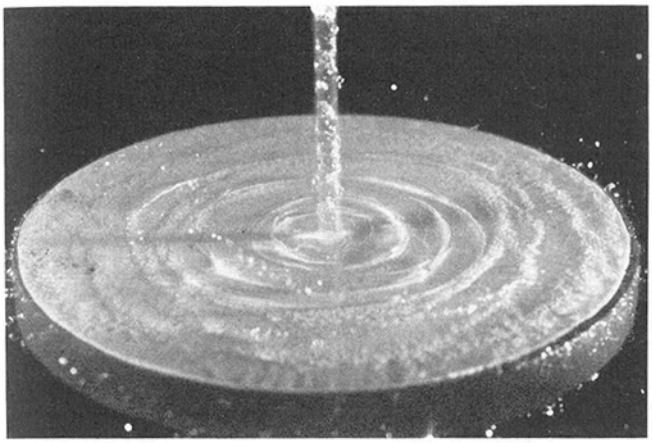

(b)

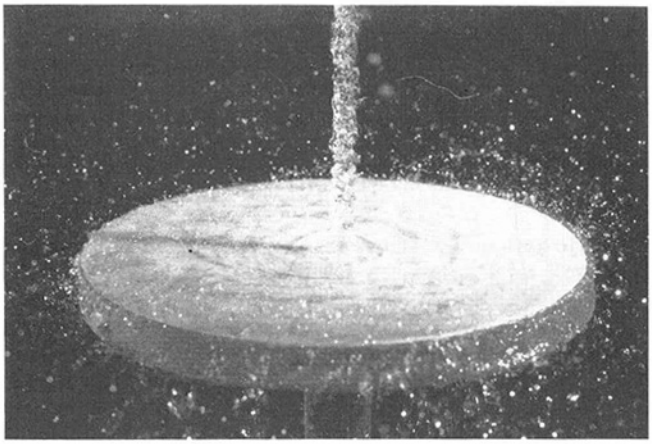

(c)

Fig. 1 (*a*) Laminar jet at $Re_d = 51{,}500$ (depth of 9.2 mm beyond hydraulic jump); (*b*) splattering jet at $Re_d = 28{,}400$, $\omega = 4550$, and $\xi = 0.108$; (*c*) splattering turbulent jet at $Re_d = 48{,}300$, $\omega = 8560$, $\xi = 0.311$ (no jump)

behavior are strongly dependent on the specific nozzle configuration, there arises the question of how best to explore the heat transfer performance of different nozzles. Most nozzle systems seek to minimize pressure drop by using a relatively large diameter liquid supply line followed by a contracting nozzle. The liquid supply may reasonably be assumed to have reached fully developed turbulent flow, and this turbulence will be partially damped by the nozzle. Actual nozzle conditions are thus bounded at one extreme by a stable laminar jet (as achieved by a sharp-edged orifice nozzle by Liu et al., 1991) and at the other extreme by a fully developed turbulent jet (as achieved by a sufficiently long tube with no outlet contraction). Other types of nozzles will generally fall between these two, having a somewhat lower turbulence intensity than in fully developed pipe flow, and their heat transfer behavior should be bounded by the laminar and fully turbulent jets.

The mean velocity profile of the jet will also affect convective heat removal, particularly in the stagnation zone. The sharp-edged orifices used in our previous studies are known to produce a uniform velocity profile about one diameter downstream of the orifice. The turbulent pipe jets studied herein have a relatively flat velocity profile as well. A recent study of planar jets (Wolf et al., 1990) concluded that velocity profile effects on stagnation zone heat transfer were pronounced for laminar flows, but suggested that, for turbulent jets, the velocity profile was relatively unimportant in comparison to the stronger influence of turbulent mixing. In this light, we expect that velocity-profile effects are less important in what follows than are the effects of turbulence. However, measurements independently varying turbulence intensity and velocity profile are needed to resolve fully the role of mean velocity profile in

Nomenclature

a = liquid jet radius
A_{rms} = mean jet-radius disturbance amplitude when jet strikes plate
C = scaled nozzle-outlet turbulence intensity = $0.195 \times \sqrt{2}(q'/u_f)^2$
C_s = const
C_f = friction factor = $\tau_w/(1/2\,\rho u_{max}^2)$
c_p = specific heat capacity per unit mass at constant pressure
d = liquid jet diameter
D = temporal volumetric mean diameter of splattered droplets at a given height
$h(r)$ = local mean thickness of liquid sheet
h_c = equivalent mean thickness of liquid sheet containing same momentum as actual sheet after splattering
h_s = mean liquid sheet thickness at the position just before splattering occurs
h^* = mean thickness of liquid sheet at the position just after splattering occurs
k = liquid thermal conductivity
l = distance between nozzle and target
Nu_d = local Nusselt number = $q_w d/k(T_w - T_f)$
p' = rms turbulent fluctuation of liquid pressure
p'_{max} = pressure disturbance amplitude at wavelength of maximum instability
Pr = liquid Prandtl number
q' = rms magnitude of turbulent velocity vector at nozzle outlet
q_w = wall heat flux, uniform
Q = total volume flow rate of jet = $\pi/4\, d^2 u_f$
Q'' = volume flow rate of splattered liquid per unit height above the plate
r = radius, measured from point of jet impact
r_m = radius of droplet profile measurement
r_s = effective radius of splattering region
R_1, R_2 = principal radii of curvature for liquid surface
Re_d = Reynolds number of the jet = $u_f d/\nu$

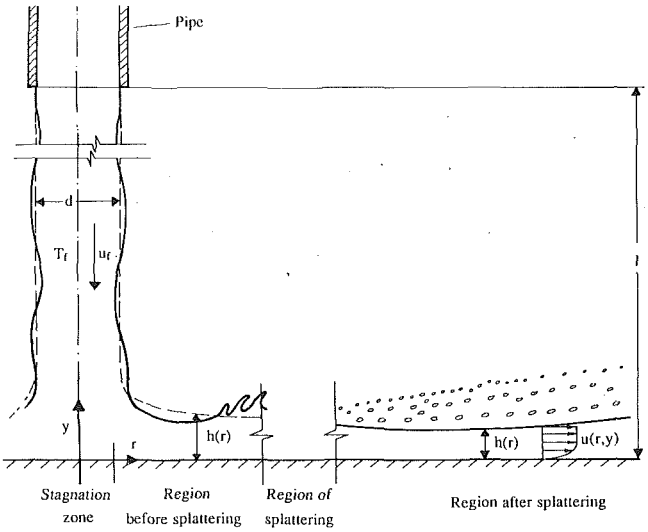

Fig. 2 Regions for turbulent incoming jet: ——— instantaneous liquid surface; --- mean liquid surface

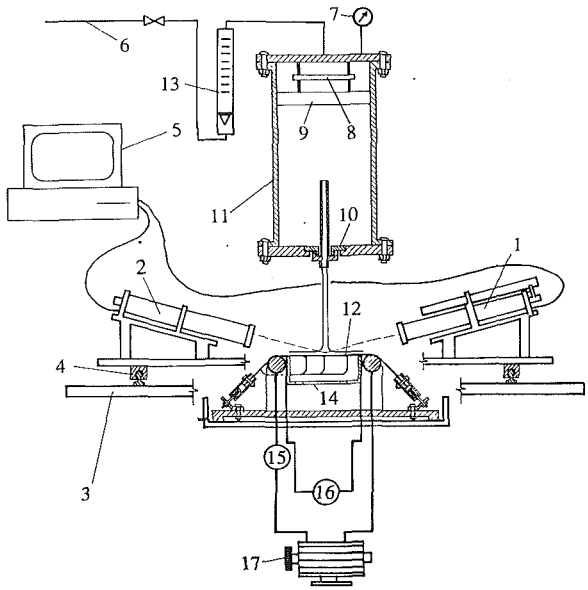

Fig. 3 Experimental apparatus: (1) PDPA laser transmitter; (2) PDPA receiver; (3) vertical traversing table; (4) horizontal rail bearings; (5) PDPA electronics; (6) water supply line; (7) pressure gage; (8) strike plate; (9) honeycomb; (10) tube support plate; (11) plenum; (12) instrumented heater sheet; (13) flowmeter; (14) insulating box; (15) electrical leads; (16) voltmeter; (17) high-current, low-voltage electric generator, 25 kW

turbulent jets, particularly for those jets having a large nonuniformity of mean velocity.

In this work, we investigate heat removal by fully turbulent liquid jets both with and without splattering. Our method is to combine relatively simple models of the mechanism of liquid splattering with phase-Doppler measurements of the splattered droplets' size and velocity to create a predictive model for the mass lost to splattering and the radial location of splatter. We then use this information to model the consequences of splattering for the efficiency of convective heat removal by the jet-induced liquid sheet, and we compare the model's results to measurements of the local Nusselt number along the wall.

Our analysis employs the momentum integral procedure, reflecting our attention to the average behavior of a physical process that is far too complex for exact analytical solution. Moreover, the momentum integral procedure has been found to facilitate relatively clear and general descriptions of the varying radial characteristics of the film flow (Liu and Lienhard, 1989); alternative, numerical procedures cannot provide any useful generality for the whole range of radius, although they show some promise for the stagnation zone (Liu et al., 1992).

2 Experiments

Experiments were performed to measure the splattered mass and heat transfer for a fully developed, turbulent liquid jet. The experimental jets were produced using long tubes (50 to 100 dia long; 3.2–9.5 mm dia), which received liquid water from a pressurized plenum and issued into still air (Fig. 3). The outlet of each pipe was carefully smoothed and deburred so that surface disturbances in the liquid jets were produced solely by the turbulence of the jets. The initial conditions for the jet should thus depend only on Reynolds number. Contraction of the turbulent jets causes less than a 1.5 percent reduction in diameter, in contrast to the large contraction for sharp-edged orifice jets. Jet velocity was determined using a flow meter (primary calibration of the meter was performed). The jets struck a thin, uniformly electrically heated plane target, which was instrumented for local temperature measurement. The nozzle to plate separation was adjustable over the

Nomenclature (cont.)

s, s_{max} = growth rate of capillary disturbances, maximum growth rate
St = local Stanton number = $q_w/(\rho c_p u_{max}(T_w - T_{sf}))$
t = time
T_f = incoming jet temperature, before impingement
$T_{sf}(r)$ = free surface temperature distribution of liquid sheet
$T_w(r)$ = wall temperature distribution
$u(r, y)$ = mean radial velocity distribution in liquid film
u_f = velocity of impinging jet (bulk velocity of flow exiting nozzle)
u_{max} = local maximum film velocity (liquid free surface velocity); mean value is near u_f in boundary layer region
u^*, u^*_{max} = liquid velocity, liquid maximum velocity just after splattering
v = mean radial velocity component of splattered droplets at a given height
We_d = jet Weber number = $\rho u_f^2 d/\sigma$
x = fraction of liquid sheet contained in boundary layer at given radius
y = distance normal to the wall
δ = viscous boundary layer thickness
ϵ, ϵ_{max} = amplitude, mean amplitude of initial surface of displacement
θ = angle in cylindrical coordinate system
Θ = constant in momentum balance, Eq. (26)
λ, λ_{max} = capillary-disturbance wavelength for jet, most unstable wavelength
ν = kinematic viscosity
ξ = ratio of splattered-liquid volume flow rate to incoming jet volume flow rate
ρ = liquid density
σ = surface tension
Φ = constant in momentum balance, Eq. (18) or (28)
ω = dimensionless group = $We_d \exp(0.971/\sqrt{We_d} \cdot l/d)$

range $1.2 \leq l/d \leq 28.7$. The remainder of the experimental apparatus consists of the water jet loop, a refrigerating system, and an electrical heating system. Full details of this equipment, the heater, the instrumentation, and the error analysis are given by Liu et al. (1991).

The distribution of the splattered droplets' velocities and diameters above the target plate were measured using a Phase Doppler Particle Analyzer (PDPA). The PDPA (Aerometrics, Inc.) is an advanced laser-Doppler velocimeter that produces concurrent measurements of an individual particle's diameter and velocity through an analysis of the measured amplitude and phase of the Doppler burst. Since the splattered droplets travel at only a small angle with respect to the target surface (about 20 deg off horizontal), the PDPA was configured to record the radial component of velocity; this component is also that required in the momentum integral analysis below. Owing to ambiguities in the instrument's probe-area correction for the number density calculation, the measured volume flux was independently calibrated by direct measurement of the splattered mass (following Errico, 1986), as shown in Fig. 4; the incoming-jet volume flow and the volume flow remaining in the liquid sheet after splattering were measured at radii corresponding to those used in the PDPA measurements.

The wall temperature increases with radius, and the local Nusselt number is based on the difference between the local wall temperature and the temperature of the incoming jets. The incoming jet temperature was measured using the stagnation point thermocouples with the heater power off (i.e., the adiabatic-wall temperature). As in our previous experiments (Liu and Lienhard, 1989; Liu et al., 1991), evaporative cooling was suppressed by limiting the maximum liquid temperature along the test heater. At the stagnation point, the temperature differences are the smallest and the uncertainty in Nusselt number is the largest when the previously mentioned heater is employed. Thus, a narrower heater strip (3.8 cm wide rather than 15.2 cm wide) was used for separate stagnation zone measurements. This enabled the use of higher heat fluxes (up to 300 kW/m^2) without concern for liquid surface temperature or burning of the test heater; the temperature differences were thus raised to accurately resolvable values for the stagnation point, providing stagnation Nusselt numbers with uncertainties of 10 percent or less. Downstream, the reported Nusselt numbers have uncertainties of only 5 percent. The estimated uncertainty for Re_d is 5 percent and that for r is 0.5 mm.

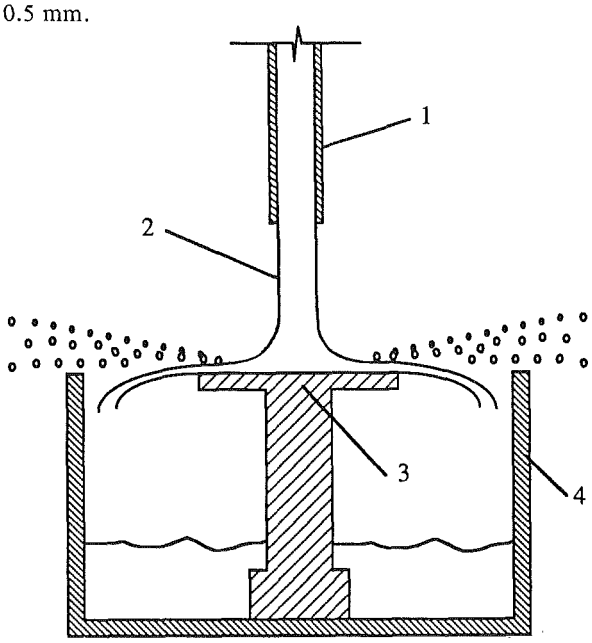

Fig. 4 Direct measurement of splattered mass: (1) tube; (2) liquid jet; (3) target disk; (4) capture tank for unsplattered liquid

Both the wide and narrow heaters were made from 0.1-mm-thick 304SS sheet. Corrections were applied for the conductive temperature difference across the Joule-heated sheet, as described by Liu et al. (1991). These corrections are quite important when Nu_d is large. Omitting them, as some authors apparently have (Faggiani and Grassi, 1990), may cause large errors.

3 Splattering

The vertical distribution of the radial volume flux of splattered droplets was measured for a variety of jet Reynolds numbers, Re_d, jet-to-plate separations, l/d, and radial measuring stations, r_m/d. Representative profiles are presented in Fig. 5(*a*); the droplet volume flow rate in the radial direction per unit height, Q'' (m^3/s m), is normalized with the total volume flow rate of the incoming jet, Q (m^3/s), and plotted as a function of the vertical distance from the plate surface at given radius. Decreasing the Reynolds number shifts the whole profile to the left. Decreasing the nozzle height has a similar effect, reducing the splattering at all vertical positions. When the profile is measured at larger radius, its basic shape changes;

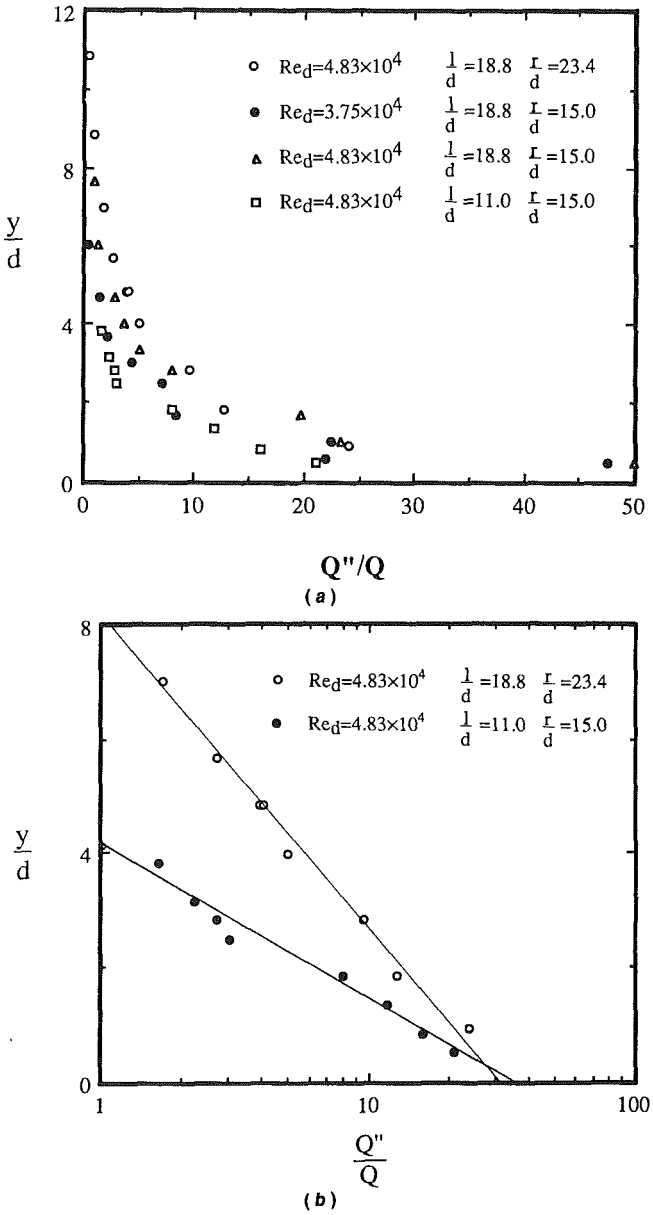

Fig. 5 Vertical distribution of splattered radial liquid volume flow rate divided by total jet volume flow rate, Q''/Q (m^{-1}): (a) linear coordinates; (b) semilogarithmic coordinates

near the wall (small y) the splattered volume flux decreases with increasing radius, but farther from the wall (larger y), the flux decreases less and may even increase. The shape distortion occurs because the droplets travel at an angle relative to the plate, and at larger radius the droplets are spread over a larger area than at small radius.

In semilogarithmic coordinates (Fig. 5*b*), the volume flux distribution is almost a straight line. A line fit may be applied to these curves, corresponding to an exponentially decaying vertical distribution of splattered mass, and the total volume flow rate of splattered droplets may then be obtained by integration. The total volume flow is then used to calibrate the volume flux measurements, as described above.

For the data shown in Fig. 5 (b), the ratio of total splattered droplet volume flow to total incoming volume flow (which is 0.34) decreases by only about 2.6 percent when the measuring radius is increased from $r_m/d=15$ to $r_m/d=24$, holding other variables constant. This difference is within the uncertainty of the measurements, although some decrease may occur as a few large droplets fall back to the liquid sheet under gravity. However, both these measurements and stroboscopic observations by Errico (1986) and by our group show that the actual splattering occurs within a certain radial band around the point of impact; beyond this band, splattering no longer occurs. Hence, the total splattered mass flow, as observed beyond the radius of splattering, will not depend on r/d, but only upon Reynolds number, Weber number, and l/d.

3.1 A Model for Splattering. The splattering of an impinging jet depends strongly upon the disturbances present on the incoming jet when it reaches the plate. These initial disturbances are sharply amplified when the fluid flows into the thin liquid film surrounding the point of impact, and their magnitude determines both whether or not the jet splatters and the magnitude of the actual splattering. The disturbances undergo substantial distortion upon entering the liquid sheet, with changes in amplitude, wavelength, and wavespeed; rigorous analysis of that development is beyond our present scope. However, we may make substantial progress by considering only the size of the disturbances that the jet delivers to the liquid sheet. Here, we present a model that relates the initial turbulence in the jet to the initial surface disturbances on the jet and their subsequent growth by capillary instability. In this way, we scale the disturbances reaching the liquid sheet that drive actual splattering.

Surface shape is related to the difference between liquid and gas phase pressure, Δp, via the Laplace relation:

$$\Delta p=\sigma\left(\frac{1}{R_1}+\frac{1}{R_2}\right) \tag{1}$$

We assume that the surface disturbances at the nozzle outlet are due primarily to turbulent pressure fluctuations within the jet, which have an rms value of

$$p'\cong\frac{1}{2}\rho(q')^2=\frac{1}{2}\rho u_f^2\left(\frac{q'}{u_f}\right)^2 \tag{2}$$

The turbulent pressure fluctuations will be distributed over a broad spectrum of wavelengths. The corresponding surface disturbances also show a range of wavelengths, some of which are more unstable than others. Rayleigh's normal mode analysis of circular jet capillary instability (Drazin and Reid, 1981) showed that a disturbance of wavelength λ evolves in time from an initial amplitude ϵ to an amplitude A given by

$$A=\epsilon\exp(i[2\pi y/\lambda+m\theta]+st) \tag{3}$$

and that the disturbance of maximum growth rate has $\lambda_{max}=4.51d$ and $m=0$. From Eq. (1), the associated initial pressure disturbance amplitude is (Drazin and Reid, 1981)

$$p'_{max}=-0.514\frac{\sigma\epsilon}{a^2} \tag{4}$$

and the corresponding growth rate may be shown to be

$$s_{max}=0.3433\sqrt{\frac{\sigma}{a^3\rho}} \tag{5}$$

Thus, if we equate the rms turbulent pressure disturbance, p', to rms capillary pressure disturbance, $|p'_{max}|/\sqrt{2}$, we obtain an rms initial surface displacement

$$\frac{\epsilon_{rms}}{a}\cong 0.781\sqrt{2}\left(\frac{\rho u_f^2 a}{\sigma}\right)\left(\frac{q'}{u_f}\right)^2 \tag{6}$$

The spectral distributions of the turbulent pressure fluctuations and the surface disturbances have been lumped into a single mean disturbance amplitude, so no direct significance should be attached to the coefficient $0.781\sqrt{2}$. However, the physical mechanism relating intensity of pressure fluctuations to the surface displacement should scale as shown irrespective of this approximation.

The liquid travels from the nozzle to the plate in a time $t=l/u_f$, during which the surface disturbance grows from the initial ϵ_{rms} to

$$A_{rms}=\epsilon_{rms}\exp(s_{max}t)=\epsilon\exp\left(0.3433\frac{l}{u_f}\sqrt{\frac{\sigma}{\rho a^3}}\right) \tag{7}$$

Nondimensionalizing yields

$$\frac{A_{rms}}{d}=C\,\mathrm{We}_d\exp\left(\frac{0.9710}{\sqrt{\mathrm{We}_d}}\frac{l}{d}\right) \tag{8}$$

where the jet Weber number is

$$\mathrm{We}_d=\frac{\rho u_f^2 d}{\sigma} \tag{9}$$

and

$$C=0.195\sqrt{2}\left(\frac{q'}{u_f}\right)^2 \tag{10}$$

Hence, the disturbance reaching the point of impact, which drives subsequent splattering, should scale with the dimensionless group

$$\omega=\mathrm{We}_d\exp\left(\frac{0.971}{\sqrt{\mathrm{We}_d}}\frac{l}{d}\right) \tag{11}$$

and the fraction of the total incoming liquid flow which is splattered, ξ, is a function of ω, which must be found experimentally.

The total turbulence intensity, q'/u_f, has an average value of approximately 0.080 in turbulent pipe flow (at $\mathrm{Re}_d=5\times10^4$) and varies only weakly with Reynolds number (roughly as $\mathrm{Re}_d^{1/8}$; Laufer, 1954; Tennekes and Lumley, 1972). The Reynolds number range of the present splattering experiments (19,000 to 69,000) is narrow enough that a constant value of $C\approx0.0018$ is an adequate initial condition for our jets. The turbulence decays under viscous influence as the jet travels to the plate; a homogeneous-turbulence decay estimate predicts a 50 percent drop in turbulence intensity if the jet is 20 diameters above the target. However, the capillary disturbances that turbulence induces at the jet outlet have grown exponentially during the journey to the target.

Figure 6 shows the ω at which we observed onset of splattering as a function of Reynolds number.[1] For all Reynolds numbers, the data show ω to be about 2120 at the onset of splattering. Thus, the jet disturbance found from the above analysis does control the stability of the liquid sheet, and ω is

[1] *Our observations were both visual and tactile; "onset" is the point at which we observed any droplets to leave the liquid sheet.*

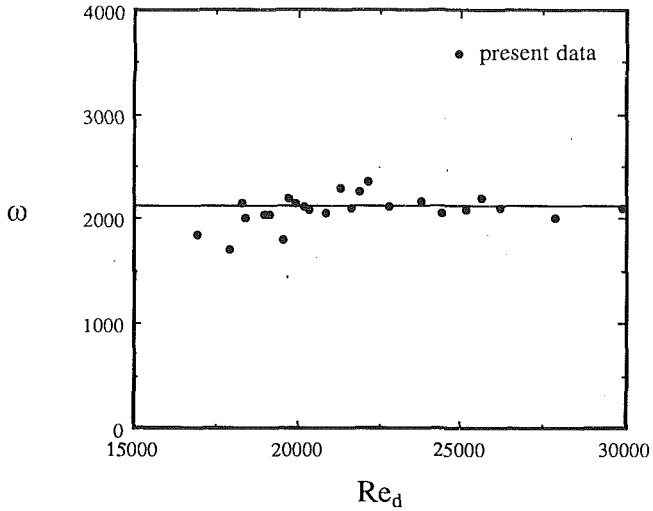

Fig. 6 The critical ω for onset of splattering as a function of Reynolds number

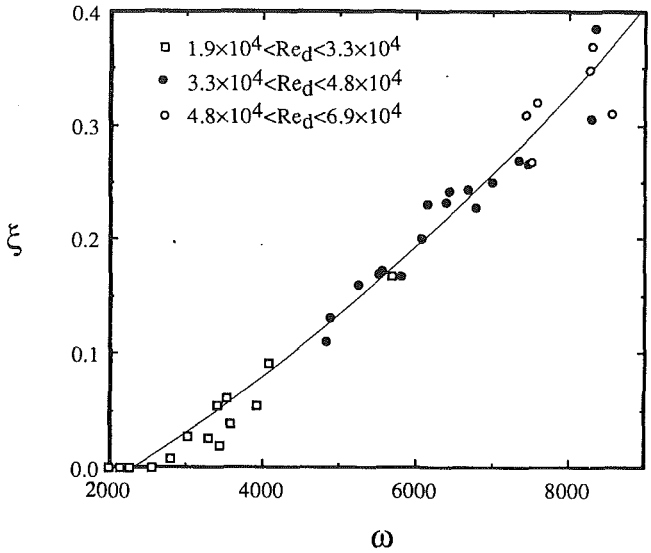

Fig. 7 The fraction of incoming mass splattered, ξ, as a function of ω; ——— curve fit

a good measure of that stability. From the definition of ω, this shows that splattering occurs whenever $We_d > 2120$, irrespective of l/d, although splattering may occur at lower values of We_d when l/d is nonzero. This graph ends at Re_d of 30,000 because our higher Re_d jets all exceeded $We_d = 2120$.

Figure 7 shows the total fraction of liquid splattered from the sheet as a function of ω. The ratio of the splattered flow to the total flow increases monotonically with ω. The amount of splattering is very small in the range $2120 \le \omega \le 3000$, with $\xi \le 2.5$ percent; in engineering applications, splattering may be neglected in this range. For $2200 \le \omega \le 8500$, splattering increases rapidly; the splattering ratio is well represented by the curve fit

$$\xi = -0.0935 + 3.41 \times 10^{-5}\omega + 2.25 \times 10^{-9}\omega^2 \qquad (12)$$

No data are available beyond $\omega = 8500$, but we can assume that ξ will flatten, since it is necessarily less than one. For these data, the uncertainty is 8 percent for ω and 1 percent for ξ.

The onset of splattering is fairly flat in the sense of ξ versus ω. Hence, the reported "onset" may vary among observers, depending on how much mass must be splattered before splattering is noticed. Few outside data are currently available for comparison to the present criterion. Womac et al. (1990) cite three observations of onset for tube nozzles 20–40 diameters in length, which may be nondimensionalized using present terminology. For water, onset was noted for a 0.978 mm nozzle at $\omega \approx 2600$–3800 with $Re_d = 13900$; for FC-77, onset was noted for a 0.978 mm nozzle at $\omega \approx 2900$–4200 with $Re_d = 5800$ and for a 0.4 mm at $\omega \approx 6600$–8300 with $Re_d = 5900$. The first pair of observations is consistent with the present results, given the smallness of ξ at those values of ω and the low (marginally turbulent) Reynolds numbers involved. The last observation is well above present results; however, the volume of splattered liquid at observed onset would have been roughly the same as for the larger nozzles, making an issue of the operating definition of "onset." From a practical viewpoint, the curve $\xi(\omega)$ itself is of greatest importance, and onset may be best defined in terms of a threshold value of ξ below which splattering can be ignored.

Bhunia and Lienhard (1992) present more detailed results for the onset of splattering and an improved version of Eq. (12).

3.2 Droplet Departure Radius. The distribution of droplet diameter, D, typically ranges from a few microns to almost a millimeter. However, most droplets passing a particular point have essentially the same velocity irrespective of their size. Very small droplets (less than about 20 μm) suffer significant

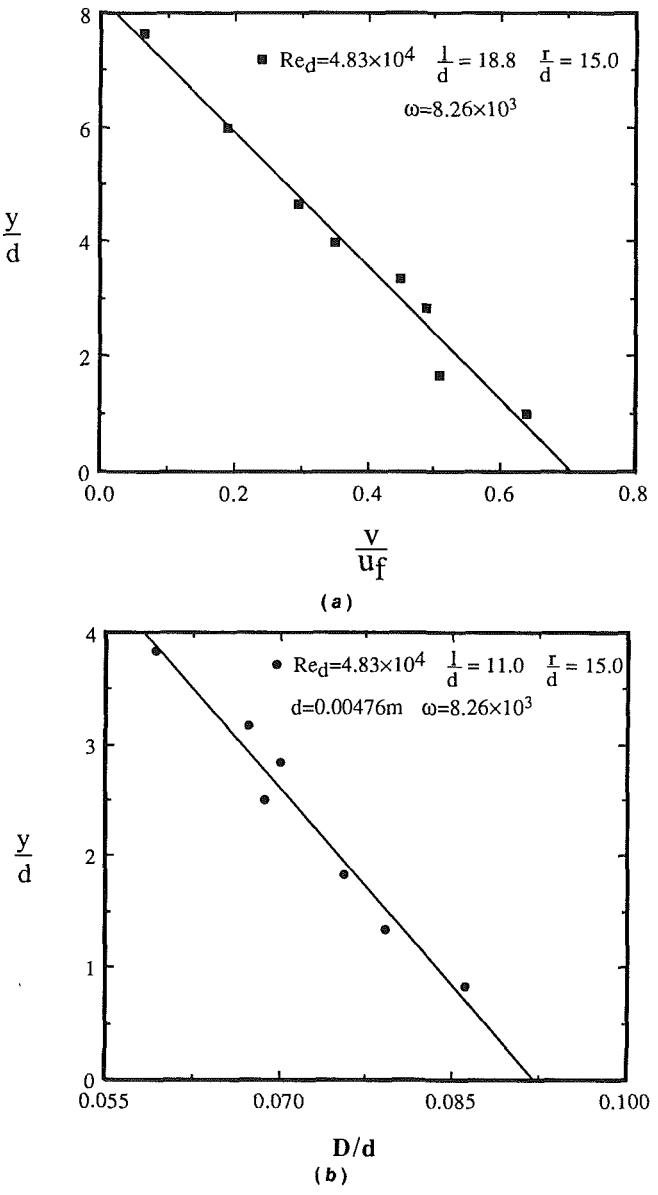

Fig. 8 (*a*) Droplet radial velocity profile above plate; (*b*) droplet diameter profile; ——— curve fits

viscous drag and move slower, but these droplets contribute little to the mass-averaged velocity. The mean droplet velocity, v, near the plate is fairly represented by a linearly decreasing velocity profile (Fig. 8*a*). The mean droplet diameter also decreases with increasing distance from the plate (Fig. 8*b*).

We may infer the radial position at which the droplets separated from the liquid surface, r_s, by assuming that the large droplets near the liquid surface maintain the radial velocity they had at the point of departure from the liquid sheet (neglecting air drag) and that the departure velocity is equal to the mean surface velocity; the droplets' velocity then determines the radial position where the liquid surface had that velocity. This estimate sets the position of breakaway at about $r_s = 5.7d$. Since the wavelength of maximum capillary instability for a circular jet is $\lambda_{max}/d = 4.51$, the estimated breakaway position is slightly more than one λ_{max}. In his experiments, Errico (1986) observed that the radius where the disturbances to the liquid sheet reach maximum height (droplet departure point) was between 0.73 cm and 1.46 cm, which appeared to be about 4 jet diameters.[2] The heat transfer data also verify this estimate indirectly, as will be discussed later. The present data do not clearly show a dependence of the breakaway radius upon Re_d, d, or ω, but more detailed measurements are unquestionably required to resolve such influences and to set a more precise value for r_s. For modeling purposes, we take $r_s \approx \lambda_{max}$ in what follows.

A few very fine droplets were observed around the incoming jet when the Reynolds number was large. These droplets appear to be generated at the jet nozzle, and are formed by a different mechanism than considered here. They have a very small contribution to the total liquid volume flow. In addition, aerodynamic drag on the jet will become increasingly important for Reynolds numbers above 50,000 and will alter the capillary growth as modeled here.

4 Mean Flow Field and Heat Transfer

For turbulent jets, and especially for those that splatter, the flow field of the liquid sheet is highly unsteady and irregular. However, for the purpose of modeling the jet heat convection, we may focus on the mean flow field and consider separately the region before splattering and the region after splattering.

Visual observation shows that the capillary disturbances create very large, highly unsteady disturbances to the liquid film. Stroboscopic observations show that the disturbances grow larger up to the point of droplet separation, where tall, sharp crests are observed; these crests break into a spray of droplets (Errico presents excellent photographs of the breakup). The capillary disturbances greatly exceed in magnitude the free-stream turbulence in the incoming jet and will promote the rapid transition to a fully turbulent film downstream.

In the region upstream of droplet breakaway, we may suppose the flow to be composed of a thin, *laminar* wall boundary layer and a turbulent, fluctuating free stream above it. We may further suppose that the capillary disturbances to the liquid surface have essentially the same effect on the boundary layer as does the free stream turbulence. This region extends to only about 5 jet diameters from the point of impact.

To gain some idea of free stream turbulence effects on wall boundary layer heat transfer, we can refer to previous studies of the problem. A general survey of free stream turbulence effects was given by Kestin (1966); the stagnation zone of a *submerged* jet was investigated numerically by Traci and Wilcox (1975). Local measurements in the laminar stagnation zone of a cylinder show an unexpectedly large effect of free stream turbulence, reaching an enhancement of more than 80 percent in $\mathrm{Nu}_d/\mathrm{Re}_d^{1/2}$ at the stagnation point for a change of turbulence intensity from 0 percent to only 2.7 percent. Laminar boundary layer heat transfer can be substantially increased if the pressure gradient is nonzero, but for zero pressure gradient (as in the present flow, *away* from the stagnation point), free-stream turbulence does not affect the local heat transfer coefficient up to a turbulence intensity of at least 3.82 percent. The turbulence intensities of these past experiments are similar to those estimated for the present case, in the absence of capillary contributions. The magnitudes of the present capillary disturbances are not known precisely; however, we compare the present measurements to the undisturbed, laminar predictions (Liu et al., 1991) below, so as to gage the magnitude of the combined turbulent and capillary augmentation.

The splattering region itself is relatively small and may be modeled as if splattering occurs at a single radius. The large disturbances associated with droplet departure may reasonably be presumed to induce fully turbulent flow in the liquid sheet after splattering. We may estimate the thickness and velocity variation of the turbulent residual sheet by accounting for the loss of mass and momentum associated with splattering. Having the velocity and thickness of the turbulent liquid sheet, we may then use the thermal law of the wall to estimate the local Nusselt number.

We emphasize that the model that follows is directed at the average behavior of the sheet, rather than a precise prediction of velocity profile and film thickness.

4.1 Mass and Momentum Conservation. At the radial location just before splattering (here taken as $r_d/d = 4.51$), the ratio of mass in the boundary layer to total incoming mass in the jet is

$$x = \frac{2\pi r \int_0^\delta u\,dy}{\frac{\pi}{4} d^2 u_f} = 13.34 \left(\frac{r_s}{d}\right)^{3/2} \mathrm{Re}_d^{-1/2} = 128.3\, \mathrm{Re}_d^{-1/2} \tag{13}$$

where, from Sharan (1984),

$$u(y) = u_f \left[\frac{3}{2}\frac{y}{\delta} - \frac{1}{2}\left(\frac{y}{\delta}\right)^3\right] \tag{14}$$

and

$$\frac{\delta}{d} = 2.679 \left(\frac{r}{d\,\mathrm{Re}_d}\right)^{1/2} \tag{15}$$

These expressions assume a laminar wall boundary layer beneath a turbulent free stream with mean velocity u_f. Stevens and Webb (1991) measured radial surface speeds for a non-splattering turbulent jet and found surface speeds near u_f (as would be expected from streamline momentum conservation); speeds up to 20 percent larger were measured for small diameter, low Reynolds number jets. As discussed below, this acceleration may be associated with surface tension effects on those small, slow jets.

If $(1-\xi) \geq x$, the splattered liquid does not include fluid in the boundary layer. In this case, the liquid sheet remaining after splattering has an effective thickness, h_c (Fig. 9), of

$$h_c = h_s - \frac{\xi d^2}{8 r_s} \tag{16}$$

where h_s is the mean film thickness prior to splattering and the second term is the loss of (inviscid) fluid due to splattering. The remaining mass flow, $(1-\xi)\pi/4 d^2 u_f$, carries momentum

$$2\pi r_s \rho \left[\int_0^\delta u^2 dy + \int_\delta^{h_c} u_f^2 dy\right] = 2\pi r_s \rho u_f^2 \Phi d \tag{17}$$

where

[2] Errico's water jet diameter was not specified, since he observed the splattering radius to be independent of jet size. From a Kelvin–Helmholtz instability analysis of the liquid sheet, Errico estimated that this radial position was one to two disturbance wavelengths.

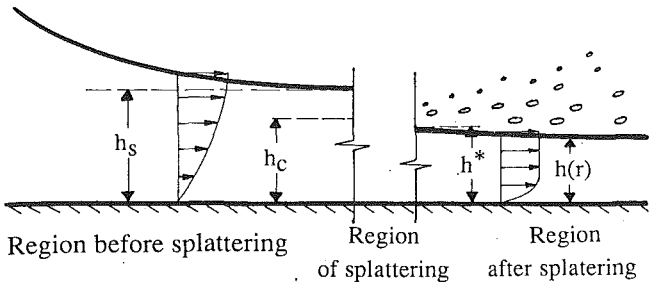

Fig. 9 Mean flow field during splattering (schematic)

$$\Phi = 0.125(1-\xi)\frac{d}{r_s} - 0.373\left(\frac{r_s}{d\mathrm{Re}_d}\right)^{1/2} \tag{18}$$

These results do not account for the transition to turbulent flow after splattering, which will change the velocity profile and alter the film thickness from h_c to another value, h^*.

Azuma and Hoshino (1984) measured the velocity distributions in the sheet for both laminar and turbulent flow; they showed that a 1/7th power law is a good approximation in the turbulent sheet:

$$u(y) = u_{\max}\left(\frac{y}{h}\right)^{1/7} \tag{19}$$

for h the thickness of the turbulent sheet and $u_{\max}$ the free surface speed. We assume the adjustment from the laminar boundary layer to turbulent sheet velocity distributions occurs within a small radial region at the zone of splattering. In terms of the turbulent thickness just after splattering, h^*, the mass flow in the sheet after splattering is

$$2\pi r_s\rho\int_0^{h^*} u\,dy = \frac{7}{4}\pi r_s\rho h^* u^*_{\max} \tag{20}$$

and the momentum flow in the sheet after splattering is

$$2\pi r\rho\int_0^{h^*} u^{*2}dy = \frac{14}{9}\pi r_s\rho h^* u^{*2}_{\max} \tag{21}$$

for u^* the mean velocity distribution in the sheet just after splattering and $u^*_{\max}$ its maximum. Then, with Eqs. (16)–(18), mass and momentum balances on the region of adjustment (at radius r_s) give

$$\frac{h^*}{d} = \frac{(1-\xi)^2 d^2}{63 r_s^2 \Phi} \tag{22}$$

At larger radii, solution of the momentum integral equation gives the variation of turbulent liquid sheet thickness as

$$\frac{h}{d} = \frac{0.02091}{[(1-\xi)\mathrm{Re}_d]^{1/4}}\left(\frac{r}{d}\right)^{5/4} + C_s\frac{d}{r} \tag{23}$$

where

$$C_s = \frac{h^* r_s}{d^2} - \frac{0.02091}{[(1-\xi)\mathrm{Re}_d]^{1/4}}\left(\frac{r_s}{d}\right)^{9/4} \tag{24}$$

Note that the above mass and momentum balances across the splattering region provided the initial conditions used in solving the momentum integral equation for $r > r_s$.

For the case $(1-\xi) < x$, the mass in the sheet after splattering is

$$(1-\xi)\frac{\pi}{4}d^2 u_f = 2\pi r\int_0^{h_c}\left(\frac{3}{2}\left(\frac{y}{\delta}\right) - \frac{1}{2}\left(\frac{y}{\delta}\right)^3\right)dy \tag{25}$$

so that

$$\frac{h_c}{\delta} \equiv \Theta = \sqrt{3 - 3\sqrt{1 - \frac{(1-\xi)d^2}{9 r_s \delta}}} \tag{26}$$

The momentum remaining within the liquid sheet is

$$2\pi r_s\rho\int_0^{h_c} u^2 dy = 2\pi r_s\rho u_f^2\delta\left(\frac{3}{4}\Theta^3 - \frac{3}{10}\Theta^5 + \frac{1}{28}\Theta^7\right) \tag{27}$$

We obtain the same results for h^* and h, Eqs. (22) and (23), except that Φ is not given as Eq. (18), but is instead

$$\Phi = \left(\frac{3}{4}\Theta^3 - \frac{3}{10}\Theta^5 + \frac{1}{28}\Theta^7\right)\frac{\delta}{d} \tag{28}$$

4.2 Heat Transfer. We may now apply the thermal law of the wall to calculate the heat transfer in the film after splattering, following Liu et al. (1991). According to the law of the wall

$$\mathrm{St} = \frac{q_w}{\rho c_p u_{\max}(T_w - T_{sf})} = \frac{C_f/2}{1.07 + 12.7(\mathrm{Pr}^{2/3} - 1)\sqrt{C_f/2}} \tag{29}$$

The friction coefficient in the liquid sheet, from the Blasius law, is

$$C_f = 0.045\left(\frac{\nu}{h u_{\max}}\right)^{1/4} \tag{30}$$

and for a turbulent sheet,

$$u_{\max} h = \frac{1}{7}\frac{u_f d^2(1-\xi)}{r} \tag{31}$$

If we define the local Nusselt number as

$$\mathrm{Nu}_d = \frac{q_w d}{k(T_w - T_f)} \tag{32}$$

then, letting $T_{sf} = T_f$ at $r = r_s$ and taking the free surface to essentially adiabatic (Liu et al.), a calculation yields

$$\mathrm{Nu}_d = \frac{8\mathrm{Re}_d\mathrm{Pr}\,\mathrm{St}}{49(hr/d^2) + 28(r/d)^2\mathrm{St}} \tag{33}$$

This expression for Nu_d may be evaluated in conjunction with Eqs. (23), (29), (30), (31), and (12).

Figure 10 shows the Nusselt number predicted above. The Nusselt number from the laminar prediction is also shown. As shown below (Figs. 13*a*, *b*), the turbulent prediction agrees reasonably well with our experimental results.

Splattering has a strong effect on heat transfer, especially immediately after the breakaway radius. Increasing the amount of mass splattered (raising ξ) deteriorates the heat transfer. Splattering thins the film, and the resultant, increased skin friction creates a rapid decay in the Nusselt number with radius. Far downstream, the heat transfer is substantially worse than for the laminar case. Similarly, as more mass is splattered (ξ increasing), the remaining film has less momentum, and slows more quickly. At radii close to the radius of splattering, however, the heat transfer is larger than for laminar flow; this results from the assumption that turbulent transition accompanies splattering. This enhancement is stronger when less mass is splattered, leaving more momentum in the film.

For the case without splattering ($\xi = 0$), the prediction and data still show an enhancement from capillary disturbances, which is caused by the turbulent transition. For $\omega < 5000$, the prediction overestimates the Nusselt number relative to measurements immediately after the "splattering" radius (19 percent higher for $\omega \approx 2400$), but farther downstream the disagreement disappears (after about $5d$ for $\omega \approx 2400$). The overprediction may occur because turbulent transition is not completed at the splattering radius; Liu et al. showed that turbulent transition can occur over a significant radial band. However, these estimates are still much closer to the data than is the laminar prediction; even in the absence of actual splattering, the liquid sheet is still highly disturbed by the capillary fluctuations.

Liu et al. (1991) showed that the stagnation zone of a uni-

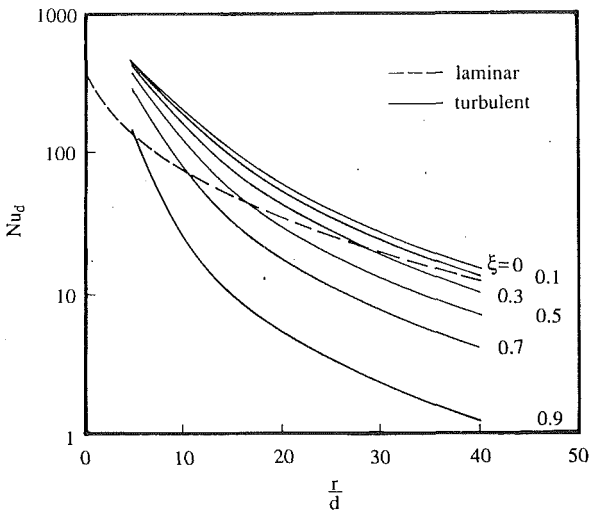

Fig. 10 Estimated Nusselt number for region after splattering as a function of fraction of mass splattered: Eq. (33); ——— ; laminar results (Liu et al.) ---

form-velocity-profile, laminar incoming jet covers the region $r/d \leq 0.787$ and that the Nusselt number there may be estimated from

$$\mathrm{Nu}_d = \begin{cases} 0.715\mathrm{Re}_d^{1/2}\mathrm{Pr}^{0.4} & 0.15 \leq \mathrm{Pr} \leq 3 \\ 0.797\mathrm{Re}_d^{1/2}\mathrm{Pr}^{1/3} & \mathrm{Pr} > 3 \end{cases} \quad (34)$$

For a turbulent incoming jet, both free stream turbulence and capillary disturbances may affect the stagnation zone heat transfer. Figure 11(*a*) shows the ratio of measured Nusselt number to $0.797\ \mathrm{Re}_d^{1/2}\mathrm{Pr}^{1/3}$ as a function of ω. The stagnation zone heat transfer appears to be essentially independent of ω. This is not surprising given that the stagnation zone is well separated from the free surface and its capillary disturbances. However, the turbulent stagnation zone heat transfer is still much higher than for a laminar impinging jet; the data show an augmentation factor of about 1.55. Turbulent disturbances are not directly separated from capillary disturbances in this presentation. However, as mentioned previously, variations in outlet turbulence intensity show only a weak additional dependence on Reynolds number beyond the u_f dependence of ω, and viscous damping of turbulence during travel to the plate may well be offset by growth of the fluctuating capillary disturbances to the fluid flow. Indeed, Fig. 11(*b*) shows the augmentation factor to be essentially independent of jet Reynolds number in this range of Re_d and ω.

The stagnation zone Nusselt number for the present experiments is represented by the following expression to an accuracy of about ±10 percent:

$$\mathrm{Nu}_d = 1.24\mathrm{Re}_d^{1/2}\mathrm{Pr}^{1/3} \quad (35)$$

This equation should apply for any Prandtl number greater than 3, although the present experiments, for $7 < \mathrm{Pr} < 11$, do not verify the Pr range.

Stevens and Webb (1989) and Jiji and Dagan (1988) present results for the turbulent stagnation zone of an unsubmerged jet. The parameter ω is generally small for both studies, given their low ranges of either Reynolds number or l/d; neither study appears to have used splattering jets. Jiji and Dagan's jets were confined to low Re_d and were produced by very short tubes, some six diameters in length. The turbulence intensity in their jets should thus be lower than for the fully developed turbulence of the present, long tubes, leading to a somewhat lower stagnation point Nusselt number. Their results are shown for comparison in Fig. 11(*a*); their data are in fact somewhat below the present data. Stevens and Webb's prediction is considered below.

For liquid jet impingement, the pressure gradient in the

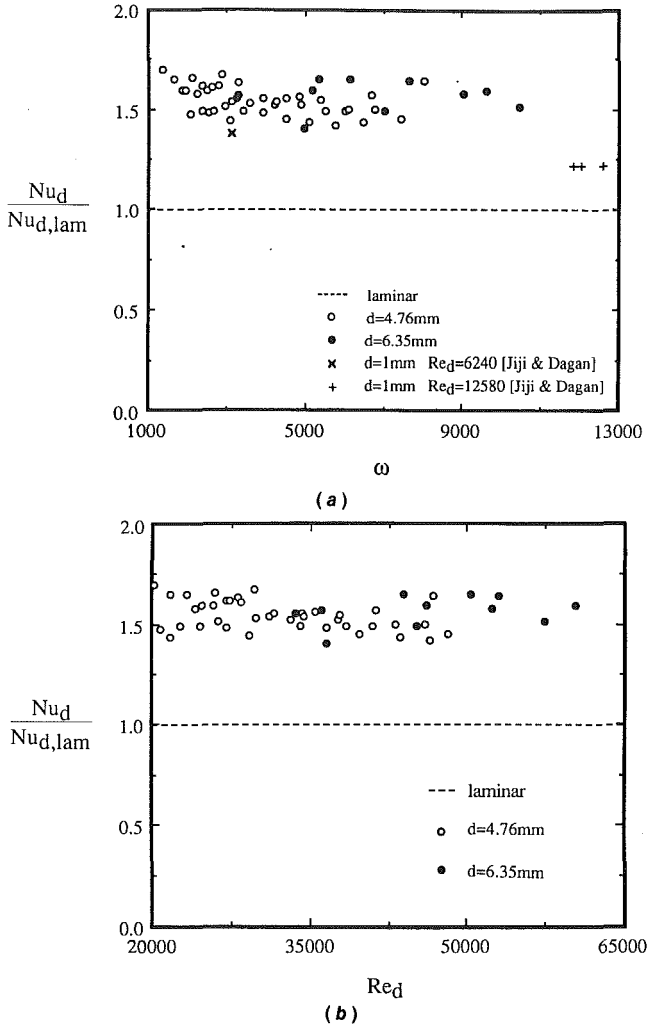

Fig. 11 Nusselt number in stagnation zone for turbulent, splattering jets relative to Nusselt number for laminar jets from Eq. (34)

region between the stagnation zone and the splattering radius is negligible, and, as noted above, previous studies (Kestin, 1966) suggest that no turbulent augmentation of the boundary layer heat transfer should occur. However, the presence of strong capillary disturbances before the radius of droplet separation provides an alternative mechanism for heat transfer enhancement. To show the effect of capillary disturbances, the Nusselt number between stagnation and splattering was averaged, and the ratio between this average Nusselt number and the averaged laminar prediction (Liu and Lienhard, 1989) was calculated. Figure 12 shows this ratio as a function of ω. The enhancement by capillary disturbances is apparent, in contrast to the stagnation zone heat transfer, and enhancement appears to be independent of Reynolds number. Capillary augmentation reaches a factor of three at $\omega = 9000$.

We may predict the Nusselt number over the entire range of radius by using Eq. (33) for the region after splattering ($r/d > 5.7$), using Eq. (35) for the stagnation zone ($r/d < 0.787$), and applying the augmentation factor (Fig. 12) to the laminar prediction between the stagnation zone and the splattering radius. This composite prediction is compared to two sets of data in Fig. 13(*a*,*b*), and the agreement is generally good. Many other cases are shown by Gabour (1991). In Fig. 13(*a*), in the region just after splattering, the data show a lower value than the prediction. The reason, as mentioned above, is that for this case ω is about 4003 and the turbulent transition is not completed in the splattering region; this disagreement disappears downstream as the transition is completed. In the figure,

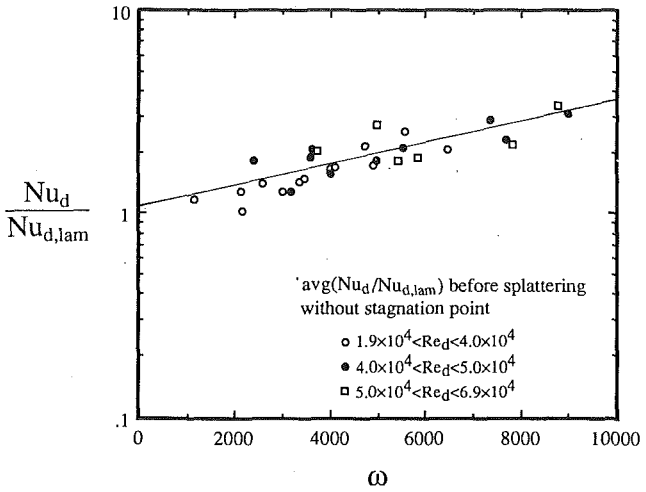

Fig. 12 Augmentation of Nu_d in boundary layer region upstream of the splattering radius as a function of ω; turbulent results normalized with laminar results of Liu and Lienhard (1989)

the correlation of Stevens and Webb (1989) underestimates the Nusselt number for $r/d>3$, consistent with its expected range of validity. Our data are somewhat higher than that correlation at small r. Figure 13(b) shows similar results at a larger ω.

5 Other Nozzles

Other nozzle configurations may have different outlet turbulence intensities. A tentative suggestion for adapting the present results to such nozzles is to rescale the present values of ω to values appropriate to such nozzles. Since the initial disturbance to the sheet is proportional to $C\omega$, the procedure is to determine the values of C and ω for the new nozzle and then find an effective value of ω as:

$$\omega_{\text{eff}} = \frac{(C\omega)_{\text{new}}}{C_{\text{present}}} \tag{36}$$

The value ω_{eff} may be used in calculations based on the present results.

Additional considerations for other nozzles include variations in the coefficient of contraction and nonuniform velocity profiles. While velocity-profile influence on heat transfer has been clearly established for laminar jets, Wolf et al. (1990) suggested that for planar, fully developed turbulent jets, the velocity profile itself has far less effect on turbulent heat transfer than does turbulence. However, measurements that independently vary turbulence intensity and mean velocity profile are needed in order to quantify and settle this issue.

Likewise, the precise effect of a nonuniform velocity distribution on the evolution of surface disturbances has yet to be clearly identified, although the present results work well for the levels of nonuniformity found in turbulent pipe jets. Until further data are obtained, a tentative recommendation is to ignore velocity profile effects on splattering, unless the nozzle produces a mean velocity profile markedly different than that for normal pipe flow.

Nonunity contraction coefficients should be taken into account when calculating jet velocity and diameter, although they seem unlikely to have a strong influence on capillary or turbulent disturbances such as are considered here. For low Reynolds number jets of small diameter, surface tension (and gravitational acceleration) can alter the flow field of the jet near the plate. Liu et al. (1992) find some evidence of such effects in the stagnation zone of laminar jets.

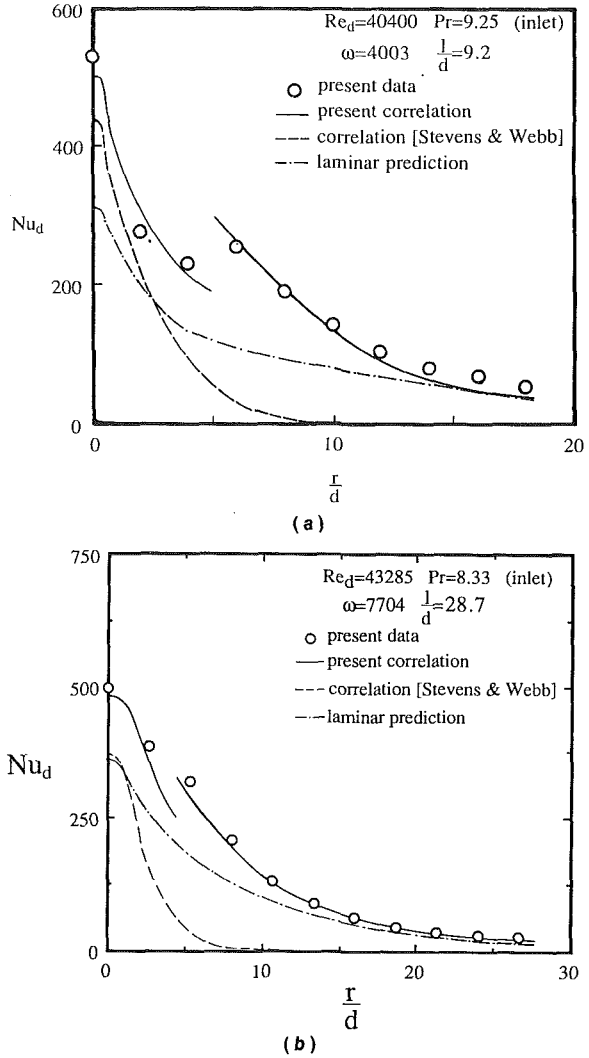

Fig. 13 Comparison of measurements to the present model: ——— from Eq. (33) and Figs. (10) and (12); laminar theory from Liu et al.

6 Conclusions

Splattering and heat transfer have been investigated for unsubmerged, circular, fully turbulent impinging liquid jets. Predictive results have been developed for the local Nusselt number along a uniform heat flux surface and for the onset of splattering and the total mass splattered.

- The occurrence of splattering is well characterized by the group ω (Eq. (11)) when: (a) the initial disturbances to the jet are produced by turbulence in the liquid exiting the nozzle; and (b) the jet Reynolds number is low enough that capillary instability guides the growth of these disturbances. The present results validate ω for $19{,}000<Re_d<69{,}000$; breakdown of the model is likely at higher Reynolds numbers due to aerodynamic drag. Differences are also expected when the turbulence is less than fully developed, as at lower Reynolds numbers. The data cover jet-to-target separations of $7.6\le l/d\le 26.4$ and $1000<We_d<5000$; the present model is likely to fail if the jet is long enough to undergo breakup prior to impact.
- Splattering occurs within a narrow radial band, rather than being distributed at all radii in the liquid sheet. The breakup radius, r_s, is about one λ_{max} (roughly $4.51d$), although further study of the scaling of both r_s and splattered droplet profiles are needed. Splattering appears to be an inviscid phenomenon.
- Jets begin to splatter when $\omega>2120$ (or for $We_d>2120$ for any l/d). The fraction of incoming mass splattered, ξ, is

given by Eq. (12) for $\omega < 8500$. These results apply for $7.6 \leq l/d \leq 26.4$ and $1000 < We_d < 5000$.

- Local Nusselt number depends on Re_d, r/d, and ω for turbulent, splattering jets. The present results facilitate prediction of local wall temperature from the stagnation zone to radii well past the splattering radius.
- Both turbulent and capillary disturbances to the free-stream flow strongly augment heat transfer in the laminar wall boundary layers in the stagnation zone and film region upstream of the splattering radius. Results are shown in Figs. 11 and 12.
- After droplet breakaway, heat transfer is further enhanced by complete turbulent transition of the viscous film. However, heat transfer drops quickly thereafter as a result of the higher skin friction in the film. Nusselt number may be estimated with Eq. (33) for $r > r_s$ and is shown in Figs. 10 and 13.
- In the stagnation zone, capillary disturbances appear to have no direct effect on the heat transfer. Augmentation by the turbulence in the incoming jet appears to increase the heat transfer by a factor of 1.55 over that for a laminar jet. Augmentation is independent of ω and Re_d over the range of those variables covered in these experiments ($1.2 \leq l/d \leq 28.7$). The stagnation zone Nusselt number ($r/d \leq 0.787$) is well represented by Eq. (35), $Nu_d = 1.24 Re_d^{1/2} Pr^{1/3}$.

Acknowledgments

The authors are grateful to Mr. John A. Simo for his assistance with the Phase Doppler equipment. This work was supported by the A. P. Sloan Foundation and the National Science Foundation under grant No. CBT-8858288. The Phase Doppler Particle Analyzer was purchased under Electric Power Research Institute contract No. RP8000-41.

References

Azuma, T., and Hoshino, T., 1984, "The Radial Flow of Thin Liquid Film, Part 3: Velocity Profile," *Trans. Japan Soc. Mech. Engrs.*, Paper No. 50-1126.

Bhunia, S. K., and Lienhard V, J. H., 1992, "Splattering of Turbulent Liquid Jets Impinging on Solid Targets: Parametric Studies," *28th AIChE/ASME Nat. Heat Transfer Conf.*, San Diego, to appear.

Drazin, P. G., and Reid, W. H., 1981, *Hydrodynamic Stability*, Cambridge University Press, United Kingdom.

Errico, M., 1986, "A Study of the Interaction of Liquid Jets With Solid Surfaces," Ph.D. Thesis, University of California, San Diego.

Faggiani, S., and Grassi, W., 1990, "Round Liquid Jet Impingement Heat Transfer: Local Nusselt Numbers in the Region With Nonzero Pressure Gradient," *Proc. Ninth Int. Heat Transfer Conf.*, Jerusalem, Vol. 4, pp. 197–202.

Gabour, L. A., 1991, "Heat Transfer to Turbulent and Splattering Impinging Liquid Jets," S.B. Thesis in Mechanical Engineering, MIT, Cambridge, MA.

Jiji, L. M, and Dagan, Z., 1988, "Experimental Investigation of Single-Phase Multijet Impingement Cooling of an Array of Microelectronic Heat Sources," *Cooling Technology for Electronic Equipment*, Hemisphere, New York.

Kestin, J., 1966, "The Effect of Free-Stream Turbulence on Heat Transfer Rates," *Adv. Heat Transfer*, Vol. 3, pp. 1–32.

Laufer, J., 1954, "The Structure of Turbulence in Fully Developed Pipe Flow," NACA Tech. Report No. 1174.

Liu, X., and Lienhard V, J. H., 1989, "Liquid Jet Impingement Heat Transfer on a Uniform Flux Surface," *Heat Transfer Phenomena in Radiation, Combustion, and Fires*, ASME HTD-Vol. 106, pp. 523–530.

Liu, X., Lienhard V, J. H., and Lombara, J. S., 1991, "Convective Heat Transfer by Impingement of Circular Liquid Jets," ASME JOURNAL OF HEAT TRANSFER, Vol. 113, pp. 571–582.

Liu, X., Gabour, L. A., and Lienhard V, J. H., 1992, "Stagnation Point Heat Transfer During Impingement of Laminar Liquid Jets: Analysis With Surface Tension," *28th AIChE/ASME Nat. Heat Transfer Conf.*, San Diego, to appear.

Lombara, J. S., 1990, "An Experimental Investigation of Liquid Jet Impingement Heat Transfer Theories," S.B. Thesis in Mechanical Engineering, MIT, Cambridge, MA.

Sharan, A., 1984, "Jet-Disc Boiling: Burnout Predictions and Application to Solar Receivers," Master's Thesis, University of Houston, TX.

Stevens, J., and Webb, B. W., 1989, "Local Heat Transfer Coefficients Under an Axisymmetric, Single-Phase Liquid Jet," *Heat Transfer in Electronics—1989*, ASME HTD-Vol. 111, pp. 113–119.

Stevens, J., and Webb, B. W., 1991, "Measurements of the Free Surface Flow Structure Under an Impinging, Free Liquid Jet," presented at the 3rd ASME/JSME Thermal Engineering Joint Conference, Reno, NV.

Tennekes, H., and Lumley, J. L., 1972, *A First Course in Turbulence*, MIT Press, Cambridge, MA.

Traci, R. M., and Wilcox, D. C., 1975, "Freestream Turbulence Effects on Stagnation Point Heat Transfer," *AIAA J.*, Vol. 13, pp. 890–896.

Wolf, D. H., Viskanta, R., and Incropera, F. P., 1990, "Local Convective Heat Transfer From a Heated Surface to a Planar Jet of Water With a Non-uniform Velocity Profile," ASME JOURNAL OF HEAT TRANSFER, Vol. 112, pp. 899–905.

Womac, D. J., Aharoni, G., Ramadhyani, S., and Incropera, F. P., 1990, "Single Phase Liquid Jet Impingement Cooling of Small Heat Sources," *Proc. Ninth Int. Heat Transfer Conf.*, Jerusalem, Vol. 4, pp. 149–154.